J|A|C|S ARTICLES

Published on Web 04/17/2009

Consequences of Acid Strength for Isomerization and Elimination Catalysis on Solid Acids

Josef Macht, Robert T. Carr, and Enrique Iglesia*

Department of Chemical Engineering, University of California at Berkeley, Berkeley, California 94720

Received February 2, 2009; E-mail: iglesia@berkeley.edu

Abstract: We address here the manner in which acid catalysis senses the strength of solid acids. Acid strengths for Keggin polyoxometalate (POM) clusters and zeolites, chosen because of their accurately known structures, are described rigorously by their deprotonation energies (DPE). Mechanistic interpretations of the measured dynamics of alkane isomerization and alkanol dehydration are used to obtain rate and equilibrium constants and energies for intermediates and transition states and to relate them to acid strength. *n*-Hexane isomerization rates were limited by isomerization of alkoxide intermediates on bifunctional metal−acid mixtures designed to maintain alkane−alkene equilibrium. Isomerization rate constants were normalized by the number of accessible protons, measured by titration with 2,6-di-*tert*-butylpyridine during catalysis. Equilibrium constants for alkoxides formed by protonation of *n*-hexene increased slightly with deprotonation energies (DPE), while isomerization rate constants decreased and activation barriers increased with increasing DPE, as also shown for alkanol dehydration reactions. These trends are consistent with thermochemical analyses of the transition states involved in isomerization and elimination steps. For all reactions, barriers increased by less than the concomitant increase in DPE upon changes in composition, because electrostatic stabilization of ion-pairs at the relevant transition states becomes more effective for weaker acids, as a result of their higher charge density at the anionic conjugate base. Alkoxide isomerization barriers were more sensitive to DPE than for elimination from H-bonded alkanols, the step that limits 2-butanol and 1-butanol dehydration rates; the latter two reactions showed similar DPE sensitivities, despite significant differences in their rates and activation barriers, indicating that slower reactions are not necessarily more sensitive to acid strength, but instead reflect the involvement of more unstable organic cations at their transition states. These compensating effects from electrostatic stabilization depend on how similar the charge density in these organic cations is to that in the proton removed. Cations with more localized charge favor strong electrostatic interactions with anions and form more stable ionic structures than do cations with more diffuse charges. Ion-pairs at elimination transition states contain cations with higher local charge density at the sp^2 carbon than for isomerization transition states; as a result, these ion-pairs recover a larger fraction of the deprotonation energy, and, consequently, their reactions become less sensitive to acid strength. These concepts lead us to conclude that the energetic difficulty of a catalytic reaction, imposed by gas-phase reactant proton affinities in transition state analogues, does not determine its sensitivity to the acid strength of solid catalysts.

1. Introduction

Deprotonation energies (DPE) are defined as the energy required to remove a proton from a neutral cluster to form the anionic conjugate base ($AH \rightarrow A^- + H^+$). Their values provide a rigorous and theoretically accessible descriptor of Brønsted acid strength, but only when the structure of the neutral acid cluster is accurately known. Keggin-type polyoxometalate (POM) clusters and zeolitic solid acids with well-defined structures allow accurate DPE estimates by electronic-structure methods and concomitant fundamental studies of the effects of acid strength on the reactivity of Brønsted acid catalysts. DPE values for structurally well-defined materials vary over a relatively broad range (113 kJ mol^{-1}), from 1087 to 1143 kJ mol^{-1} for Keggin-type polyoxometalate (POM) clusters ($H_{8-n}X^{n+}W_{12}O_{40}$; $H_{8-n}XW$)[1] with different central atoms, X (P, Si, Al, and Co; in order of increasing DPE), and from 1171 to 1200 kJ mol^{-1} for zeolites Y, CHA, MOR, ZSM5 (in order of decreasing DPE).[2,3]

We have recently shown that 2-butanol dehydration rate constants are larger on POM clusters than on H-BEA zeolites, consistent with the lower DPE values of POM clusters, which indicate that POM clusters are stronger acids than zeolites.[1,4] Elimination rate constants depend exponentially on DPE for several alkanol dehydration and ether cleavage reactions on $H_{8-n}XW$ POM clusters and H-BEA zeolites.[1,4] This dependence is consistent with rigorous Born−Haber thermochemical cycles, which show that the energy of kinetically relevant carbenium-

(1) Macht, J.; Janik, M. J.; Neurock, M.; Iglesia, E. *Angew. Chem., Int. Ed.* **2007**, *46*, 7864.
(2) Brändle, M.; Sauer, J. *J. Am. Chem. Soc.* **1998**, *116*, 5428.
(3) Lo, C.; Trout, B. *J. Catal.* **2004**, *227*, 77.
(4) Macht, J.; Janik, M. J.; Neurock, M.; Iglesia, E. *J. Am. Chem. Soc.* **2008**, *130*, 10369.

10.1021/ja900829x CCC: $40.75

ion type elimination transition states depends on: (i) the DPE of the acid catalyst; (ii) the energy of the reaction of a proton with the gas-phase alkanol to form water and a carbenium-ion complex, in a structure that resembles the late transition states involved; and (iii) the electrostatic ion-pair interaction energy at the transition state.[4]

We address here whether transition state energies can also be treated in this manner for alkene isomerization on structurally well-defined Brønsted acids and, by inference, for Brønsted acid catalysis in general. We report the effects of DPE on elementary rate constants for isomerization elementary steps, which limit bifunctional alkane isomerization rates on POM clusters with different central atoms and on zeolite H-BEA. We extract these fundamental kinetic parameters from alkane reactions on physical mixtures of these solid acids with Pt/Al_2O_3, which is used to maintain constant and known concentrations of alkene intermediates during catalysis.

We show that isomerization rate constants increase monotonically with decreasing DPE on POM catalysts as their central atoms increase in valence. These constants are much lower on H-BEA, a weaker acid with a larger DPE value than POM clusters. These trends are consistent with the involvement of carbocations[5] as transition states in kinetically relevant skeletal isomerization steps. We also address here the elusive and controversial issues related to how reactions catalyzed by Brønsted acids "sense" the strength of the acid sites involved. We do so by comparing the effects of DPE on rate constants for elementary isomerization and alkanol dehydration steps and show that reactions with higher activation barriers or lower rate constants are not necessarily more sensitive to acid strength than less demanding reactions. The sensitivity of reactions to acid strength depends on the structure of intermediates leading to the kinetically relevant transition state and on the charge distribution and mode of interaction with anionic clusters at these transition states. These properties define the relation between deprotonation energy and ion-pair stabilization energy, as we have shown earlier for elimination reactions.[4] The energies of transition states weakly stabilized by electrostatic interactions depend more sensitively on acid strength than those of more effectively stabilized transition states, whose charge distribution and charge separation resemble those of the proton removed during deprotonation and thus recover a larger fraction of the energy required for proton transfer to reactants.

2. Experimental Methods

2.1. Catalyst Synthesis. $H_3PW_{12}O_{40}$ (Aldrich), $H_4SiW_{12}O_{40}$ (Aldrich, 99.9%), $H_5AlW_{12}O_{40}$ (prepared as reported in ref 6), and $H_6CoW_{12}O_{40}$ (prepared as described in refs 7, 8) clusters were supported on SiO_2 (Cab-O-Sil, 304 $m^2\ g^{-1}$, 1.5 $cm^{-3}\ g^{-1}$ pore volume; washed three times in 1 M HNO_3 (Aldrich, 99%) and treated in flowing dry air (Praxair, UHP, 573 K, 5 h, 20 $cm^3\ g^{-1}$)) by incipient wetness impregnation of their respective solutions (1.5 cm^3 ethanol (Aldrich, anhydrous 99.5%) per g of dry SiO_2). These samples were held in closed vials to ensure that redistribution of POM clusters led to uniform spatial concentration profiles[9] and were then treated in flowing dry air (Praxair, UHP, 20 $cm^3\ g^{-1}$) at 323 K for 24 h.

^{31}P NMR confirmed the structural integrity of the supported POM clusters for H_3PW/SiO_2, indicating that deposition procedures did not decompose the POM clusters.[4] The nomenclature used throughout lists the surface density (as POM nm^{-2}) before the respective compositions in abbreviated form (e.g., $H_3PW_{12}O_{40} \rightarrow H_3PW$; $0.04H_3PW/Si$). The surface density for samples used in most of the data reported here (0.04 POM nm^{-2}) corresponds to a 5.5 wt % POM content.

Pt/Al_2O_3 (1.5 wt % Pt) cocatalysts used in alkane isomerization studies were prepared by first treating γ-Al_2O_3 (Sasol North America Inc., Lot # C1643, 193 $m^2\ g^{-1}$, 0.57 $cm^3\ g^{-1}$ pore volume) in flowing dry air (Praxair, 99.99%, 0.8 $cm^3\ g^{-1}\ s^{-1}$) to 923 K for 3 h (0.083 K s^{-1}). Pt was deposited by incipient wetness impregnation with aqueous chloroplatinic acid (Aldrich, CAS #16941-12-1). Samples were dried in ambient air at 383 K for at least 8 h and treated in flowing dry air (Praxair, 99.99%, 0.7 $cm^3\ g^{-1}\ s^{-1}$) to 823 K (0.083 K s^{-1}) for 3 h to decompose the precursors. Treatment in H_2 (Praxair, 99.99%, 3.3 $cm^3\ g^{-1}\ s^{-1}$) was carried out at 723 K (0.083 K s^{-1}) for 2 h. After being cooled in He (Praxair, UHP, 3.3 $cm^3\ g^{-1}\ s^{-1}$), reduced Pt/Al_2O_3 was treated at 303 K in a mixture of dry air (Praxair, 99.99%) in He (Praxair, UHP) (0.1 air/He molar ratio, 3.3 $cm^3\ g^{-1}\ s^{-1}$) to passivate Pt cluster surfaces and prevent uncontrolled oxidation upon exposure to ambient air. The Pt dispersion (60.1%) was determined by H_2 chemisorption at 313 K (Quantasorb analyzer; Quantachrome Corp.) using 1:1 H:Pt stoichiometry. Physical mixtures of $H_{8-n}X^{n+}W/SiO_2$ with Pt/Al_2O_3 were prepared by grinding mixtures with the desired ratio of surface Pt to total H^+ (given by the POM stoichiometry) (Pt/H^+); these mixtures, consisting of the cocatalysts present as small aggregates ($<10\ \mu$m diameter) were then pressed into wafers, crushed, and sieved to retain 125−180 μm aggregates.

2.2. Hexane Isomerization Rate Measurements. Catalytic measurements were carried out at 453−503 K in a tubular quartz flow reactor (1.0 cm inner diameter; 0.1−0.4 g of catalyst). Samples were held onto a porous quartz disk and heated to 473 at 0.083 K s^{-1} in flowing He (0.83 $cm^3\ s^{-1}$) before catalytic measurements. Temperatures were measured using a K-type thermocouple located within a dimple at the external quartz wall of the reactor and controlled (±0.2 K) using a Watlow controller (Series 982) and a resistively heated furnace. Transfer lines were held at 393 K to prevent adsorption or condensation of reactants and products, and also of titrants used to measure the number of Brønsted acid sites during catalysis. *n*-Hexane (Sigma-Aldrich, 99%, Fluka, 99%) was used without additional purification and introduced as a liquid using a syringe pump (Cole Parmer, 74900 series) by vaporization at 333 K into flowing He (Praxair, UHP) and H_2 (Praxair, UHP). Molar flow rates of He, H_2, and *n*-hexane were adjusted to give the desired *n*-hexane and H_2 pressures and space velocities and to maintain nearly constant low conversions (1−5%). Reactant and product concentrations were measured by gas chromatography using flame ionization detection (Agilent 6890N GC, 50 m HP-1 column). 2-Methylpentane and 3-methylpentane were the predominant reaction products, and the 2-methylpentane to 3-methylpentane ratio was 1.44−1.54. Smaller alkanes (C_1−C_5) formed with low selectivity (1.6−3.7%); the preponderance of methane and ethane among smaller products indicates that such products reflect hydrogenolysis instead of cracking pathways.

Rates decreased slightly with time at the highest *n*-hexane/H_2 molar ratios in our experiments; rate data at these conditions were corrected using

$$\Theta(t) = \Theta_0 \exp\left(\frac{-k_{deact}K_{prot}K_{dehy}^2(nC_6/H_2)^2 t}{1 + K_{prot}K_{dehy}(nC_6/H_2)}\right) \quad (1)$$

(5) Boronat, M.; Viruela, P.; Corma, A. *J. Phys. Chem.* **1996**, *100*, 16514.
(6) Cowan, J. J.; Hill, C. L.; Reiner, R. S.; Weinstock, I. A. *Inorg. Synth.* **2002**, *33*, 18.
(7) Baker, L. C. W.; McCutcheon, T. P. *J. Am. Chem. Soc.* **1956**, *78*, 4503.
(8) Baker, L. C. W.; McCutcheon, T. P. *J. Am. Chem. Soc.* **1950**, *72*, 2374.
(9) Lee, S. Y.; Aris, R. *Catal. Rev.-Sci. Eng.* **1985**, *27*, 207.

where $\Theta(t)$ and Θ_0 are the number of accessible protons at a given time and initially, respectively. This equation was derived by assuming that deactivation occurs by oligomerization of linear hexene isomers with adsorbed hexoxide species. The deactivation constant k_{deact} and the alkoxide formation equilibrium constant (K_{prot}) (vide infra) were determined from time on stream behavior at different (nC_6/H_2) molar ratios and isomerization rates as a function of (nC_6/H_2) molar ratios, respectively, by returning to reference conditions throughout the experiment. These corrections were small (<20%). The alkane dehydrogenation constant (K_{dehy}) was calculated from thermodynamic tables.[10]

Brønsted acid sites were titrated during bifunctional alkane isomerization catalysis by introducing 2,6-di-*tert*-butylpyridine (Aldrich, 97%) dissolved in *n*-hexane into He/H_2 streams at 373 K to give a mixture containing *n*-hexane (3 kPa) and 2,6-di-*tert*-butylpyridine (1.4 Pa). The amount of titrant adsorbed on the catalyst was determined from its residual concentration in the effluent using chromatographic protocols similar to those used for catalytic reactions.

2.3. Alkanol Dehydration Rates and Selectivities. Rates and selectivities were measured at 333−413 K using the experimental setup described in section 2.2 for *n*-hexane isomerization. Alkanol reactants (Sigma-Aldrich, 99.5% (2-butanol), 99.8% (1-butanol)) were used without additional purification and introduced as a liquid using a syringe pump (Cole Parmer, 74900 series) by vaporizing it into flowing He (Praxair, UHP) at 393 K. The molar rates of He and all gaseous species were adjusted to give the desired reactant pressures and to maintain low and relatively constant reactant conversions (<10%). Reactant and product concentrations were measured by gas chromatography using flame ionization detection (Agilent 6890N GC, 50 m HP-1 column). Alkenes were the main products detected (>99% 1-butene, *cis*-2-butene, *trans*-2-butene) during 1-butanol and 2-butanol dehydration. Brønsted acid sites were titrated by introducing pyridine (Aldrich, 99.9%) dissolved in 2-butanol reactants (Sigma-Aldrich, 99.5%, anhydrous) into flowing He and vaporized at 373 K to give a stream containing 0.5 kPa 2-butanol and 0.9 Pa pyridine. The amount of titrant adsorbed on the catalyst was determined using the chromatographic protocols described above.

2.4. Theoretical Calculations and Methods. Density functional (DFT) calculations were performed using the Gaussian 03 program.[11] Geometries were optimized and energies calculated at the B3LYP/6-31+G(d,p) level of theory. The DPE values of Keggin-type POM clusters with different central atoms have been previously reported.[1,4,12] Atomic charges were calculated using the Mulliken population analysis[13] as implemented in the Gaussian 03 program. Only changes in charge distribution but not the absolute values of the charges, which show a strong basis-set dependence,[14] were of interest in our theoretical analysis.

3. Results and Discussion

3.1. Kinetics and Elementary Steps for *n*-Hexane Isomerization on POM Clusters and H-BEA. *n*-Hexane (nC_6) isomerization rates and selectivities were measured on catalysts containing both metal and acid functions, because monofunctional acid-catalyzed pathways are limited by initiation steps involving alkene formation, often catalyzed by redox or impurity sites unrelated to the number or strength of Brønsted acid sites.

Table 1. First-Order *n*-Hexene Isomerization Rate Constants ($k_{isom}K_{prot}$) (cf., Eq 2 and Scheme 1) for Physical Mixtures of $0.04H_3PW/Si$ and 1.5 wt % Pt/Al_2O_3 and Coimpregnated $Pt/0.04H_3PW/Si$ with Different Pt/H^+ Ratios (473 K)

catalyst	(Pt/H^+) ratio	relative[a] first-order *n*-hexene isomerization rate constant ($k_{isom}K_{prot}$)
physical mixtures of H_3PW/Si and 1.5 wt % Pt/Al_2O_3	0.1	0.72
	0.2	1.11
	1	1
coimpregnated $Pt/0.04H_3PW/Si$	1	0.96

[a] Normalized by the first-order rate constant of the H_3PW/Si−1.5 wt % Pt/Al_2O_3 physical mixture sample with a (Pt/H^+) ratio of 1. 95% confidence intervals of the regression are <±15% of the reported values for the first-order rate constants.

The temperatures required for these initiation steps (>573 K) often lead to structural degradation of POM clusters. Also, alkene isomerization reactions proceeding after initiation via adventitious alkene impurities or intrinsic protolytic dehydrogenation reactions cause significant alkene concentration gradients along the catalyst bed, reaction dynamics that cannot be interpreted mechanistically, and alkene oligomerization and concomitant formation of unreactive residues (see also section 2.2). In contrast, bifunctional alkane isomerization strategies,[15] involving intimate mixtures of metal and acid functions, maintain low and constant equilibrium alkene concentrations at acid sites, when, as in this study (vide infra), the metal function is present at concentrations required to maintain alkane−alkene equilibria.

Table 1 shows that first-order *n*-hexene isomerization rate constants (normalized by their value at a surface Pt atom to acid site ratio (Pt/H^+) of 1) do not depend on Pt/H^+ ratios in the catalyst mixture for values greater than 0.2. These data show that these Pt contents are sufficient to maintain alkane dehydrogenation steps at equilibrium throughout the catalyst. At the (Pt/H^+) ratios of unity used throughout this study, the concentration of alkene intermediates is determined exclusively by alkane−alkene thermodynamics and does not depend on the Pt/H^+ ratios in catalyst mixtures. First-order rate constants were similar on a physical mixture of Pt/Al_2O_3 with H_3PW/SiO_2 (the catalyst with the highest volumetric isomerization rates) and on H_3PW/SiO_2 samples onto which Pt was coimpregnated at the same Pt/H^+ ratio as in the mixtures (∼1; Table 1). Thus, we conclude that transport artifacts and concomitant intraparticle alkene concentration gradients, which would be most severe for physical mixtures and for the most active acid catalysts, did not corrupt the kinetic character of the rates reported here.

Figure 1 shows *n*-hexane isomerization rates (per accessible proton; from titration during catalysis) on H_4SiW/SiO_2 and H-BEA (both as mixtures with Pt/Al_2O_3) as a function of (nC_6/H_2) reactant molar ratios. Reaction rates increased with increasing (nC_6/H_2) ratio, linearly at first and then more gradually, on POM and H-BEA catalysts (Figure 1). The reciprocal of the isomerization rates depends linearly on (H_2/nC_6) ratios on all catalysts (Figure 2). These data are consistent with the sequence of elementary steps that we discuss next.

Scheme 1 shows elementary steps involved in the acid-catalyzed part of bifunctional isomerization sequences, together with quasi-equilibrated dehydrogenation steps catalyzed by the metal function. These steps describe the relevant chemistry on mixtures of Pt/Al_2O_3 with $H_{8-n}X^{n+}W/SiO_2$ or H-BEA acids.

(10) Stull, D. R.; Westrum, E. F.; Sinke, G. C. *The Chemical Thermodynamics of Organic Compounds*; Robert E. Krieger Publishing Co.: Malabar, 1987.
(11) Frisch, M. J.; *Gaussian 03*, revision C.02; Gaussian, Inc.: Wallingford, CT, 2004.
(12) Janik, M. J.; Kimberly, A. C.; Bardin, B. B.; Davis, R. J.; Neurock, M. *Appl. Catal., A* **2003**, 256–51.
(13) Mulliken, R. S. *J. Chem. Phys.* **1962**, *36*, 3428.
(14) Wiberg, K. B.; Rablen, P. R. *J. Comput. Chem.* **1993**, *14*, 1504.
(15) Weisz, P. B.; Swegler, E. W. *Science* **1957**, *126*, 31.

Scheme 1. Proposed Mechanism for *n*-Hexane Isomerization on Bifunctional Metal−Brønsted Acid Catalysts

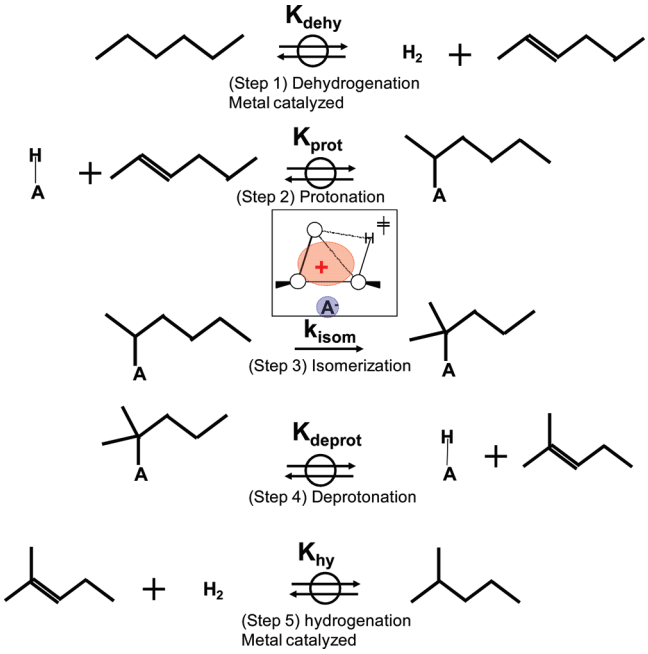

n-Hexane dehydrogenates on Pt sites to form all linear hexene isomers (Scheme 1, step 1), which are protonated on Brønsted acid sites to form the respective alkoxides (Scheme 1, step 2). Alkoxides then isomerize via edge-protonated dialkyl cyclopropane transition states[5,16,17] to form monobranched alkoxide isomers (Scheme 1, step 3), which desorb via deprotonation to form isoalkenes (Scheme 1, step 4). These isoalkenes hydrogenate via quasi-equilibrated steps on Pt (Scheme 1, step 5) to complete the bifunctional alkane isomerization cycle. This proposal is consistent with previous studies of alkane isomerization on mixtures of Pt/Al_2O_3 and $Cs_xH_{3-x}PW_{12}O_{40}$ (x = 1.5−2.5).[18,19]

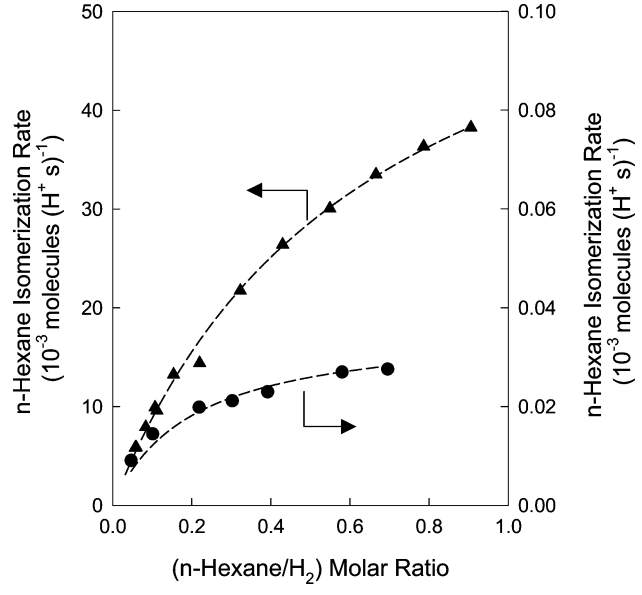

Figure 1. *n*-Hexane isomerization rates (per H^+) as a function of (nC_6/H_2) ratio for physical mixtures of $0.04H_4SiW/Si-Pt/Al_2O_3$ (▲) and $H-BEA-Pt/Al_2O_3$ (●) (473 K, $Pt/H^+ = 1$). The dashed lines represent fits to the experimental data using eq 2. 95% confidence intervals for regression parameters, k_{isom} and K_{prot}, used to make the dashed lines are <±11% of their values.

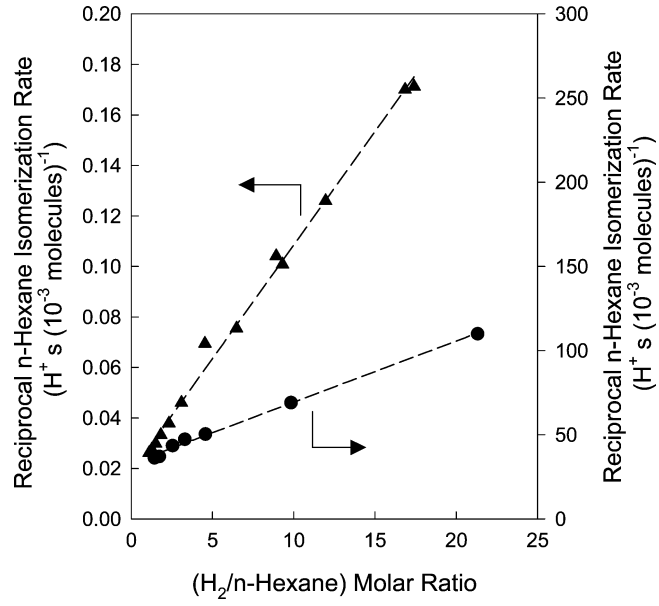

Figure 2. Reciprocal *n*-hexane isomerization rates (per H^+) as a function of (H_2/nC_6) ratio for physical mixtures of $0.04H_4SiW/Si-Pt/Al_2O_3$ (▲) and $H-BEA-Pt/Al_2O_3$ (●) (473 K, $Pt/H^+ = 1$). Dashed lines represent linear fits of the data shown. 95% confidence intervals for regression parameters, k_{isom} and K_{prot}, used to make the dashed lines are <±11% of their values.

Scheme 2. Branching Rearrangement of the Linear Secondary Carbenium Ion (2-Hexenium Ion) (A) with the Edge-Protonated 1-Ethyl-3-methyl Cyclopropane Carbocation Transition State (B) to the Monobranched 2-Methyl 3-Pentenium Ion (C)[a]

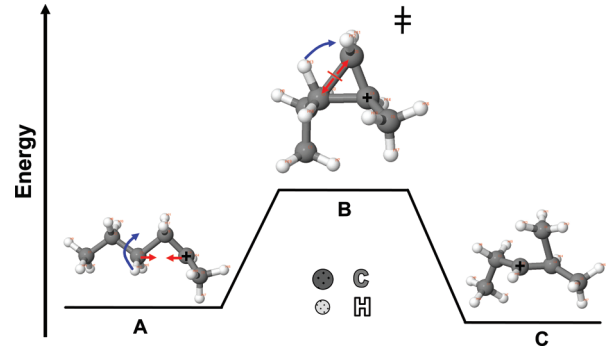

[a] The branching step involves the concerted C−C and C−H bond cleavage and formation. The transition state (B) is likely to resemble the transition state of the isomerization step catalyzed by a Brønsted acid (cf., Scheme 1, step 3).

Isomerization involves concerted reactions of C−C and C−H bonds via cationic transition states (Scheme 2B) that resemble edge-protonated dialkyl-cyclopropyl species. Such transition states involve partial formation and cleavage of C−C bonds, elongation of C−H bonds (Scheme 2), and three-carbon structures coplanar with the H-atom in elongated C−H bonds. Branching rearrangements of linear secondary carbenium ions in the gas phase (Scheme 2A) give 2-methyl 3-pentenium cations

(16) Demuth, T.; Rozanska, X.; Benco, L.; Hafner, J.; van Santen, R. A.; Toulhoat, H. *J. Catal.* **2003**, *214*, 68.
(17) East, A. L.; Bucko, T.; Hafner, J. *J. Phys. Chem. A* **2007**, *111*, 5945.
(18) Liu, Y.; Koyano, G.; Misono, M. *Top. Catal.* **2000**, *11/12*, 239.
(19) Travers, C.; Essayem, N.; Delage, M.; Quelen, S. *Catal. Today* **2001**, *65*, 355.

(Scheme 2C) via such transition states (Scheme 2). These transition states resemble those proposed from theoretical treatments for *n*-pentene isomerization on MCM-22 zeolites.[16] The specific details of this transition state are not essential to interpret isomerization rate data, but become important later as we assess the different sensitivities of isomerization and alkanol dehydration to acid strength (section 3.5).

Quasi-equilibrated alkane hydrogenation−dehydrogenation steps on Pt sites (Scheme 1, steps 1 and 5) and alkene protonation−alkoxide deprotonation steps on acid functions (Scheme 1, steps 2 and 4), together with kinetically relevant alkoxide isomerization steps (Scheme 1, step 3) and pseudo steady-state concentrations for all adsorbed species, lead to the equation:

$$r_{isom} = \frac{k_{isom}K_{prot}K_{dehy}\dfrac{[nC_6]}{[H_2]}[H^+]}{1 + K_{prot}K_{dehy}\dfrac{[nC_6]}{[H_2]}} \quad (2)$$

which is consistent with all isomerization rate data. Similar equations were used to describe bifunctional *n*-alkane isomerization rates on Pt-zeolites[20] and other catalysts.[21] Analysis of rate data based on this equation allows estimates of rate and equilibrium constants for catalysts with different acid strength.

In eq 2, k_{isom} is the rate constant for kinetically relevant alkoxide isomerization steps (Scheme 1, step 3), K_{prot} is the equilibrium constant for *n*-alkoxide formation by protonation of alkenes (Scheme 1, step 2), K_{dehy} is the equilibrium constant for the alkane dehydrogenation reaction (available from thermodynamic data), and $[H^+]$ is the number of protons accessible during catalysis, measured here by titration with 2,6-di-*tert*-butylpyridine during catalysis (see Figure 3 and Table 2 for titration data). Equation 2 is consistent with the observed linear dependence of reciprocal isomerization rates on (H_2/nC_6) reactant ratios (Figure 2). Values for $k_{isom}[H^+]$ and K_{prot} (K_{dehy} from thermodynamic tables[10]) were estimated by regression of rate data to the form of eq 2. 95% confidence intervals for these regressed parameters are $<\pm 11\%$ of the reported values. The predicted *n*-hexane isomerization rates (dashed curves in Figure 1) from eq 2 and the regressed constants ($k_{isom}[H^+]$ and K_{prot}) accurately describe all measured rate data.

Equation 2 indicates that accurate estimates of rate ($k_{isom}[H^+]$) and equilibrium (K_{prot}) constants require (nC_6/H_2) ratios that cause detectable contributions from the second term in its denominator and, as a result, lead to kinetically detectable alkoxide coverages. At such conditions, alkoxide reactions with alkenes can form unreactive oligomers, often implicated in kinetic inhibition or site blockage during acid catalysis. The slow and slight deactivation detected at higher (nC_6/H_2) ratios was rigorously taken into account by correcting rates using control measurements at a reference (nC_6/H_2) ratio at various times (as described in section 2.2).

3.2. 2,6-Di-*tert*-butylpyridine Titration during *n*-Hexane Isomerization. The intrinsic rate constant, k_{isom}, in eq 2 can only be obtained, however, when $[H^+]$ values can be measured independently. These values can be determined during isomerization catalysis by titration of active Brønsted acid sites with 2,6-di-*tert*-butylpyridine. Figure 3 shows *n*-hexane isomerization rates on $H_4SiW/SiO_2-Pt/Al_2O_3$ mixtures as a function of time on stream before titrant injection and then as a function of the cumulative amount of titrant adsorbed. 2,6-Di-*tert*-butylpyridine was used instead of more polar pyridine titrants, because the latter can access protons within POM secondary structures,[22] which are inaccessible to nonpolar hexene reactants. *n*-Hexane isomerization rates decreased almost linearly as 2,6-di-*tert*-butylpyridine decreased the number of Brønsted acid sites. The number of titrants required to suppress isomerization rates was 2.2 titrants per POM cluster on $H_4SiW/SiO_2-Pt/Al_2O_3$ (Figure 3). *n*-Hexane isomerization rates reached undetectable levels during titration; thus, either all sites accessible to reactants are also accessible to 2,6-di-*tert*-butylpyridine or irreversible titrant adsorption renders any residual protons either inaccessible or unreactive. The latter was suggested by DPE estimates that increase upon coadsorption of electron donors; coadsorption concurrently increased DFT estimates of alkanol dehydration activation barriers on H_3PW and H_5AlW POM clusters.[23] We cannot rule out that 2,6-di-*tert*-butylpyridine irreversibly titrates inactive protons, which would make the number of sites measured an upper bound, but the presence of such protons is unlikely in well-defined POM cluster structures.

Titrant uptakes during alkane isomerization were larger on $0.04H_4SiW/Si$ (2.2 per POM) than on $0.04H_3PW/Si$ (1.4 per

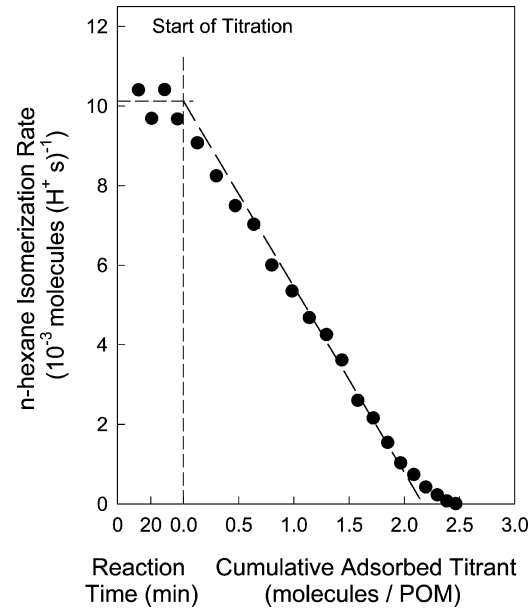

Figure 3. Titration of acid sites on a physical mixture of $0.04H_4SiW/Si-Pt/Al_2O_3$ ($(Pt:H^+) = 1$) during *n*-hexane isomerization at 473 K. Reaction rates (per H^+) as a function of the cumulative amount of titrant (2,6-di-*tert*-butylpyridine) adsorbed during reaction (0.1 (nC_6/H_2) ratio, 3 kPa *n*-hexane, 1.4 Pa 2,6-di-*tert*-butylpyridine). 95% confidence intervals on cumulative titrant uptakes are $<\pm 5\%$ of the reported values.

Table 2. 2,6-Di-*tert*-butylpyridine Uptake (per POM) Measured by Titration during *n*-Hexane Isomerization Reaction (cf., Figure 3)

	2,6-di-*tert*-butylpyridine uptake (molecules per POM)[a]
$0.04H_3PW/Si$	1.4
$0.04H_4SiW/Si$	2.2 (cf., Figure 3)
$0.04H_5AlW/Si$	2.0

[a] 95% confidence intervals on uptake values are $<\pm 5\%$ of the reported values.

(20) van de Rundstraat, A.; Kamp, J. A.; Stobbelaar, P. J.; van Grondelle, J.; Krijnen, S.; van Santen, R. A. *J. Catal.* **1997**, *171*, 77.
(21) Djéga-Mariadassou, G.; Boudart, M. *J. Catal.* **2003**, *216*, 89.
(22) Macht, J.; Carr, R. T.; Iglesia, E. *J. Catal.*, accepted.
(23) Janik, M. J.; Macht, J.; Iglesia, E.; Neurock, M. *J. Phys. Chem. C* **2009**, *113*, 1872.

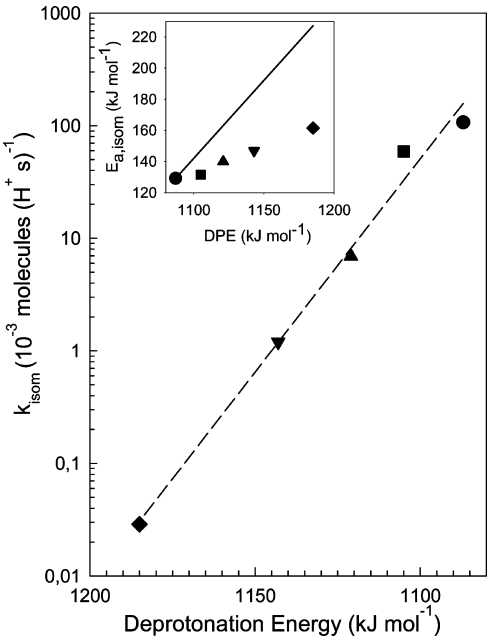

Figure 4. *n*-Hexane isomerization rate constant k_{isom} (Scheme 1, step 3) as a function of deprotonation energy, defined as ΔE_{rxn} of HA → A^- + H^+ (noninteracting) (HA is the acid, and A^- is the conjugate base) and calculated by DFT for physical mixtures of $0.04H_3PW/Si$ (●), $0.04H_3SiW/Si$ (■), $0.04H_5AlW/Si$ (▲), and $0.04H_6CoW/Si$ (▼) and H-BEA (◆) and Pt/Al_2O_3 (473 K, Pt:H^+ = 1). k_{isom} values were obtained by fitting eq 2 to the kinetic data (see also Figure 2) and normalization by the 2,6-di-*tert*-butylpyridine uptake, which corresponds to the number of accessible protons. The inset shows the isomerization activation barriers as a function of DPE. 95% confidence intervals for k_{isom} from regression are <±6.5% of the reported values.

POM) and similar on $0.04H_4SiW/Si$ and $0.04H_5AlW/Si$ (2 per POM). These uptakes are smaller than expected for fully protonated POM clusters (3.0 per POM for $0.04H_3PW/Si$) (Table 2) and have errors <±5% of the reported values. Supported POM clusters can form cubic secondary structures, and in the absence of polar molecules, 2,6-di-*tert*-butylpyridine titrates only protons at their external surfaces, but not internal protons, which are also inaccessible to nonpolar reactants during isomerization catalysis.[24] Smaller titrant uptakes than stoichiometric values may also reflect protons that become inaccessible or unreactive as a result of H-bonding with hydroxyls on SiO_2 surfaces. Measured titrant uptakes (per POM) are larger than unity on all samples; thus, POM clusters are well-dispersed, and most protons are accessible to nonpolar titrants and reactants. These conclusions are consistent with transmission electron micrographs that detect predominantly isolated clusters and two-dimensional POM structures on these samples.[22]

3.3. Effects of Acid Strength on *n*-Hexane Isomerization and Alkanol Dehydration Activation Barriers Catalyzed by $H_{8-n}X^{n+}W/SiO_2$ and H-BEA. Figure 4 shows *n*-hexane isomerization rate constants (k_{isom}) on $H_{8-n}X^{n+}W$ (X = P^{5+}, Si^{4+}, Al^{3+}, and Co^{2+}) and on H-BEA (all as physical mixtures with Pt/Al_2O_3) as a function of deprotonation energies (DPE).[1] These k_{isom} values decreased exponentially with increasing DPE values (decreasing acid strength), as in the case of alkanol dehydration reactions.[1,4] These exponential trends indicate that DPE values,

(24) For bulk H3PW (6 m^2 g^{-1} surface area), a 2,6-di-*tert*-butylpyridine uptake of 1.1 nm^{-2}, corresponding to monolayer coverage, was measured in the presence of nonpolar *n*-hexane, while an uptake of 11 nm^{-2}, much higher than monolayer coverage, was measured in the presence of the polar 2-butanol reactant.

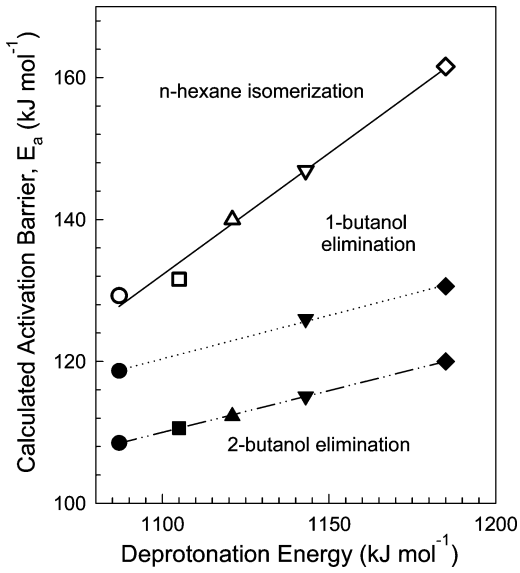

Figure 5. 1-Butanol and 2-butanol dehydration (full symbols) and *n*-hexane isomerization (open symbols) activation barriers as a function of deprotonation energy. Activation barriers were calculated from pre-exponential factors (Table 4) and experimentally measured rate constants on $0.04H_3PW/Si$ (●), $0.04H_4SiW/Si$ (■), $0.04H_5AlW/Si$ (▲), and $0.04H_6CoW/Si$ (▼) and H-BEA (◆) for alkanol dehydration and as physical mixtures with Pt/Al_2O_3 for *n*-hexane isomerization.

Table 3. Pre-exponential Factors (A_i) and Activation Barriers (E_{ai}) for 2-Butanol and 1-Butanol Dehydration and *n*-Hexane Isomerization Reactions

catalyst	reaction	A_i (s^{-1})	E_{ai} (kJ mol^{-1})
$0.04H_3PW/Si$	2-butanol dehydration	2×10^{15}[a]	108[a]
	1-butanol dehydration	7×10^{14}	119
	n-hexane isomerization	2×10^{13}	129

[a] See also ref 4 for 1- and 2-butanol dehydration activation barriers.

and by inference acid strength, predominantly influence activation barriers instead of pre-exponential factors for kinetically relevant isomerization elementary steps, a conclusion consistent with the thermochemical cycle formalism described below. Pre-exponential factors for 2-butanol dehydration were similar ($(1.5-1.9) \times 10^{15}$ s^{-1}) on Keggin POM clusters with different DPE values (1087−1121 kJ mol^{-1}), confirming the predominant influence of DPE and acid strength on activation barriers.[4]

n-Hexane isomerization activation barriers were calculated from measured rate constants on $H_{8-n}X^{n+}W/SiO_2$ and H-BEA catalysts (Figure 4, inset) using pre-exponential factors measured on $0.04H_3PW/SiO_2$ (2×10^{13} s^{-1}). These barriers are shown as a function of DPE in Figure 4 together with the line expected if activation barriers changed with catalyst composition by the same amount as DPE values ($d(E_a)/d(DPE) = 1$; Figure 4, inset). Measured barriers give slopes smaller than unity, indicating that compensating factors dampen the DPE effects on activation barriers. We address this in section 3.5 using thermochemical cycles that assess how specific catalyst properties determine the stability of the relevant transition states.

Figure 5 shows that activation barriers for alkanol dehydration (1- and 2-butanol) and *n*-hexane isomerization (Table 3) depend differently on DPE, indicating that compensating factors are specific to a given chemical reaction and that more difficult reactions are not necessarily more sensitive to acid strength than are less demanding ones (as discussed in section 3.5). For instance, 2-butanol dehydration activation barriers increased by 6 kJ mol^{-1} as DPE increased by 56 kJ mol^{-1} from H_3PW to

Table 4. Estimated Alkoxide Formation Enthalpies (ΔH_{prot}) (from the Experimental Alkoxide Formation Equilibrium Constants K_{prot} (See also Figure 6)) and the Partition Function Calculated for the Formation of a Secondary Hexoxide Species from *trans*-2-Hexene and H_2SO_4 (A_{prot}) for H_3PW_{12} and H-BEA[a]

	H_3PW_{12}	H-BEA
K_{prot} (Pa^{-1})	4	22
A_{prot}	5.5×10^{-8}	
ΔS_{prot} (J (K mol^{-1}))	−139	
estimated ΔH_{prot} (kJ mol^{-1})	−116	−122

[a] The vibrational partition function was calculated using the vibrational frequencies estimated by DFT.

Scheme 3. Thermochemical Cycle for Acid−Base Reactions over Brønsted Acid Catalysts[a]

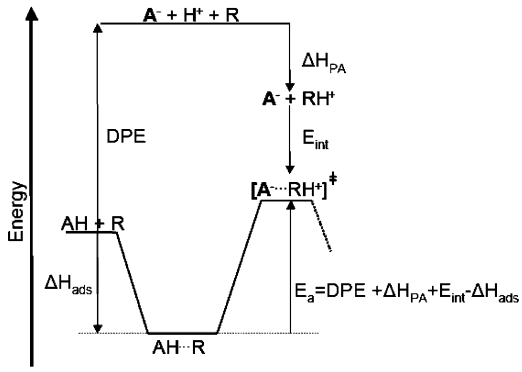

[a] The barrier (E_a) is determined by the deprotonation energy (DPE) of the acid (AH), the proton affinity (ΔH_{PA}) (cf. eqs 4 and 5), the ion-pair interaction energy (E_{int}), and the reactant adsorption enthalpy (ΔH_{ads}).

H_6CoW. The corresponding slope (0.11) in Figure 5 is very similar to that for 1-butanol dehydration (0.13), which proceeds via much less stable primary carbenium ions and with much higher activation barriers, but is much smaller than the slope for isomerization barriers (0.32).

We consider next how DPE influences acid catalysis using the formalism of Born−Haber thermochemical cycles to describe the stability of transition states based on the properties of reactants and catalysts.[4,25] Such cycles exploit the thermodynamic nature (and path independence) of the relevant energies for reactants, intermediates, and transition states. These treatments apply in general to acid catalysis, but are specifically used here for isomerization and elimination elementary steps involving ion-pairs at their transition states. The cycle in Scheme 3 indicates that activation barriers (E_a) for acid-catalyzed steps depend on catalyst deprotonation energies (DPE), "proton affinities" (ΔH_{PA}), interaction energies between cations and anions at the transition state (E_{int}), and reactant adsorption enthalpies (ΔH_{ads}):

$$E_a = \mathrm{DPE} + \Delta H_{PA} + E_{int} - \Delta H_{ads} \quad (3)$$

ΔH_{PA} depends only on the identity of the reactant and on the specific chemical rearrangement considered, because it applies to a reaction between gas-phase reactants and free protons, for which catalyst properties are inconsequential. This hypothetical gas-phase rearrangement forms the cationic moiety at the transition state, which resembles a protonated reactant for early transition states, a protonated product for late transition states, or in the case of isomerization, a species lying along the reaction coordinate from protonated reactants to products. For the late transition states involved in alkanol dehydration, the relevant gas-phase reaction is:

$$\mathrm{ROH} + \mathrm{H}^+ \rightarrow \mathrm{R}^+ + \mathrm{H_2O} \quad (4)$$

in which R denotes an alkyl fragment. This "proton affinity" accounts for the sensitivity of elimination activation barriers to the identity of the alkanol reactants. It reflects the stability of carbenium ions at transition states, which depends strongly on the degree of substitution at the carbon atoms predominantly bearing the positive charge.[4] The corresponding reaction for isomerization is:

$$\mathrm{R} + \mathrm{H}^+ \rightarrow \mathrm{RH}^+_{prop} \quad (5)$$

in which RH_{prop}^+ is an edge-protonated dialkyl-cyclopropyl species (Scheme 2B). We have calculated the structure of this isomerization transition state (edge-protonated dialkyl-cyclopropyl species, Scheme 2B) and the ΔH_{PA} term for the gas-phase branching rearrangement of a linear secondary carbenium ion (protonated reactant) (Scheme 2A) to form 2-methyl 3-pentyl cations (protonated product) (Scheme 2C) using DFT methods (section 2.4). The energy of this transition state relative to the 2-hexene and proton reactants, which gives ΔH_{PA} for *n*-hexane isomerization (eq 5), is −770 kJ mol^{-1}.

Transition states inferred from DFT treatments show that the cation structure depends sensitively on the stability of the respective isolated cations.[16,23] Alkanol dehydration transition states on Keggin clusters resemble the protonated gas-phase products (carbenium ion and H_2O),[23] while those for *n*-pentene isomerization on H-ZSM-22[16] lie along the reaction coordinate between protonated reactants and products (edge-protonated dialkyl-cyclopropyl species) and consist of a structure analogous to that obtained from our DFT simulations. Thus, gas-phase transition states do not undergo large structural rearrangements upon interaction with the catalyst. Such rearrangements would need to be included in E_{int} of the thermochemical cycle (eq 3) along with the electrostatic interactions.

Both E_{int} and ΔH_{ads} terms involve interactions between the reactant and the inorganic catalyst; consequently, they depend on the identity of both. E_{int} reflects electrostatic interactions in transition state ion-pairs and depends on the charge distributions in isolated and interacting conjugate base anions and in organic cationic fragments. This transition state is typically preceded by an adsorbed species; thus, we must also account for the energy of these species relative to the gas-phase reactant(s) (ΔH_{ads}). These adsorbed precursors involve hydrogen bonding for alkanol dehydration and alkoxide species from gas-phase alkenes for isomerization. Alkanol adsorption energies may sense acid strength because H-bonds involve partial transfer of the proton to the alkanol. In contrast, ΔH_{ads} for alkoxide formation involves covalent and van der Waals interactions that stabilize bound reactants as neutral species (section 3.4). Their interactions would sense acid strength differently from charged species and perhaps not at all, as we discuss next.

3.4. Alkoxide Formation and Stability on $H_{8-n}X^{n+}W/SiO_2$ and H-BEA. Measured alkene protonation equilibrium constants (K_{prot}; from rate data and eq 2) increased slightly with increasing DPE values (Figure 6), indicating that weaker acids (with higher DPE) tend to form slightly more stable alkoxides. These findings are consistent with conclusions from previous DFT treatments of alkoxides on Keggin-type POM clusters.[23] The basis for these weak effects of acid strength on alkoxide stability remains unclear, because effects of acid strength are expected and evident for ion-pair stability,[4] but not for alkoxide−conjugate-base

(25) Aronson, M. T.; Gorte, R. J.; Farneth, W. E. *J. Catal.* **1986**, *98*, 434.

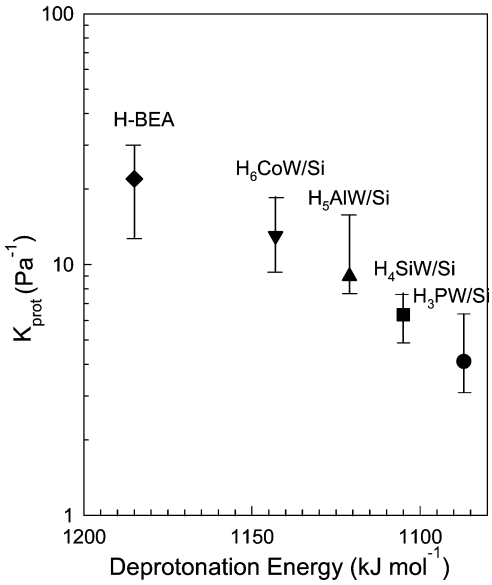

Figure 6. Equilibrium constant for alkoxide formation K_{prot} (Scheme 1, step 2) as a function of deprotonation energy, defined as ΔE_{rxn} of HA → $A^- + H^+$ (noninteracting) (HA is the acid, and A^- is the conjugate base) and calculated by DFT for physical mixtures of $0.04H_3PW/Si$ (●), $0.04H_4SiW/Si$ (■), $0._5AlW/Si$ (▲), and $0._6CoW/Si$ (▼) and H-BEA (◆) and Pt/Al_2O_3 (473 K, $Pt:H^+ = 1$). K_{prot} values were obtained by fitting eq 2 to the kinetic data (see also Figure 2) and dividing the parameter $K_{prot}K_{dehy}$ by the dehydrogenation equilibrium constant K_{dehy}. The vertical lines show the uncertainty of the K_{prot} estimates (at 95% confidence).

complexes, which are stabilized via covalent bonds instead of electrostatic interactions between organic cations and inorganic anions.[26]

The enthalpy of alkoxide formation ($\Delta H_{prot} \equiv \Delta H_{ads}$) in eq 3 (step 2 in Scheme 1):

$$C_6H_{12} + HOM \leftrightarrow H_{13}C_6OM \quad \Delta H_{prot} \tag{6}$$

(HOM denotes the acid) reflects differences in energies (BE) among the (σ) C−OM bond formed, the H−OM bond broken, the C−H bond formed in alkyl fragments, and the π-bond broken in alkene reactants. They also include a nonspecific energy term (ΔH_{ns}) that accounts for weak van der Waals interactions between the organic and inorganic fragments in the alkoxide−cluster complex:

$$\Delta H_{prot} = BE(\sigma C{-}H) + BE(\sigma C{-}OM) - BE(\sigma H{-}OM) - BE(\pi C{=}C) + \Delta H_{ns} \tag{7}$$

van der Waals interactions are not included in bond energies[27] but are especially relevant for adsorbed species and transition states within small zeolite channels.[28] The values of BE(σC−OM), BE(σH−OM), and ΔH_{ns} depend on the inorganic acid and may lead to differences in ΔH_{prot} among acid catalysts. ΔH_{prot} values become more negative as DPE values increase. Acids with a given inorganic structure, such as $H_{8-n}X^{n+}W$ POM clusters (or zeolites), have similar contributions from nonspecific van der Waals interactions (ΔH_{ns}). Therefore, higher K_{prot} values on weaker acids must reflect a systematic increase in the (positive) difference between BE(σC−OM) and BE(σH−OM). van der Waals interactions are stronger (ΔH_{ns} is more negative) on H-BEA than on isolated POM clusters, because curvature within small channels provides more effective van der Waals contacts between molecules and framework oxygens.[26] Differences in ΔH_{prot} values among different catalysts reflect differences in both bond energies (BE(σC−OM), BE(σH−OM)) and nonspecific interaction enthalpies; thus, simple correlations with DPE, evident for cationic intermediates or transition states, would be unexpected for covalently bound alkoxides.

The deconvolution of alkoxide formation energies using eq 7 is more appropriate than that using eq 3, because DFT treatments indicate that alkoxide formation energies on H_3PW do not correlate with carbenium ion stabilities or DPE values.[29] Calculated energies for 1-butene conversion to *sec*-butyl alkoxides (−102.6 kJ mol^{-1}) are more negative than for isobutene conversion to *tert*-butyl alkoxide (− 91.4 kJ mol^{-1}), even though ΔH_{PA} values for isobutene (−844.5 kJ mol^{-1}),[30] which forms a tertiary *tert*-butyl carbenium ion, are more negative than for 1-butene, which forms a secondary carbenium ion (−808.9 kJ mol^{-1}).[29,30] Similar trends have been reported for 1-butene and isobutene protonation on ferrierite.[31]

The deprotonation energies for the three distinct oxygen sites in H_3PW POM clusters are 1077, 1079, and 1071 kJ mol^{-1}.[32] *sec*-Butoxide formation energies (from 1-butene) on these three positions are −102.6 kJ mol^{-1} for the terminal oxygen atom and −79.7 and −36.2 kJ mol^{-1} for the two bridging sites; these values do not correlate with the respective DPE values for protons at these two sites, but are influenced instead by the value of the BE(σC−OM) term in eq 7.[29] Shorter alkoxide C−O bonds form on terminal oxygens because of weaker steric hindrance; C−O bonds in *sec*-butyl alkoxides are also shorter than those in *tert*-butyl alkoxides, consistent with the strong influence of steric hindrance on alkoxide stability. The covalent nature of bound alkoxides accounts for the weak effects of DPE on ΔH_{prot}, which depends instead on catalyst properties unrelated to acid strength.

The isomerization adsorption enthalpies in the thermochemical treatment (Scheme 3; eq 3) were estimated from K_{prot} values derived from *n*-hexane isomerization rate data using eq 2 (4−22 Pa^{-1} at 473 K; Figure 6, Table 4). These values were used together with pre-exponential factors (A_{prot}) estimated for secondary hexoxide formation. These A_{prot} values were calculated for *trans*-2-hexene reactions with gas-phase H_2SO_4 clusters to form secondary hexoxides using statistical mechanics[33] and scaled vibrational frequencies[34] (from DFT), including hindered rotations[35] ($A_{prot} = 5.5 \times 10^{-8}$ atm^{-1}, Table 4). These estimates led to ΔH_{prot} values between −116 to −122 kJ mol^{-1} on $H_{8-n}X^{n+}W/Si$ ($X = P^{5+}$, Si^{4+}, Al^{3+}, and Co^{2+}) and H-BEA. The ΔH_{prot} value obtained from temperature effects on K_{prot} values for H_3PW/Si was −118 kJ mol^{-1}, in agreement with ΔH_{prot} estimates from measured K_{prot} values and calculated pre-exponential factors (−116 kJ mol^{-1}). These ΔH_{prot} values on H_3PW/Si (−116 kJ mol^{-1}) differ from DFT estimates for *sec*-butoxide formation from *trans*-2-butene on H_3PW (−79.9 kJ mol^{-1}),[29] even though both involve *sec*-alkoxides. These differences reflect the recognized limitations in most DFT treat-

(26) Kazansky, V. B. *Acc. Chem. Res.* **1991**, *24*, 379.
(27) Here, bond enthalpies are for the reaction of, for example, $HO^\bullet + H^\bullet \rightarrow H_2O$ (ΔH_{rxn}); they are therefore negative values.
(28) Eder, F.; Lercher, J. A. *J. Phys. Chem. B* **1997**, *101*, 1273.
(29) Campbell, K. A.; Janik, M. J.; Neurock, M.; Davis, R. J. *Langmuir* **2004**, 21–4738.
(30) Janik, M. J.; Davis, R. J.; Neurock, M. *Catal. Today* **2005**, *105*, 134.
(31) Nieminen, V.; Sierka, M.; Murzin, D. Y.; Sauer, J. *J. Catal.* **2005**, *231*, 393.
(32) Janik, M. J.; Campbell, K. A.; Bardin, B. B.; Davis, R. J.; Neurock, M. *Appl. Catal., A* **2003**, *256*, 51.
(33) Hill, T. L. *An Introduction to Statistical Thermodynamics*; Dover Publications, Inc.: New York, 1986.
(34) Scott, A. P.; Random, L. *J. Phys. Chem.* **1996**, *100*, 16502.
(35) Ayala, P. Y.; Schlegel, H. B. *J. Chem. Phys.* **1998**, *108*, 2314.

ments of van der Waals interactions,[31,36] which stabilize adsorbed species and cause DFT methods to underestimate adsorption energies.[31]

ΔH_{prot} values from measured K_{prot} values and A_{prot} estimates for *n*-hexene on H-BEA (−122 kJ mol^{-1}; Table 1, Figure 4) are less negative than previously measured (−140 kJ mol^{-1}).[37] These differences may reflect the fact that actual A_{prot} values may be smaller than our estimates, because of larger entropy losses upon adsorption within constrained environments, where internal rotations and vibrations may be hindered as compared to those in the gas-phase *n*-hexene−H_2SO_4 complexes used to calculate vibrational modes for adsorbed 2-hexoxides (Table 4). Both measured[37] and estimated (Table 4) ΔH_{prot} values are more negative on H-BEA than on POM acids, because of more effective van der Waals contacts for alkoxides within zeolite channels (i.e., a more negative ΔH_{ns} term in eq 3)[22] and perhaps also as a result of smaller differences between σC−OM and the σH−OR bond enthalpies in eq 7. It is likely that adsorbed reactants and transition states are affected equally by increased nonspecific interactions and steric constraints in zeolite channels so that activation barriers and DPE for H-BEA coincide with the correlation for Keggin POM.

3.5. Sensitivity of Catalytic Reactions of Alkanes and Alkanols to Acid Strength. We next address the factors responsible for the compensation effects that cause activation barriers to vary by less than the change in DPE values as acid strength varies with catalyst composition (Figure 4, inset) and, more generally, for the sensitivity of catalytic reactivity to acid strength (Figure 5). The slopes in Figure 5 reflect the total derivative of activation barriers, given by the thermochemical cycles in section 3.3 (eq 3), with respect to DPE:

$$\frac{d(E_a)}{d(DPE)} = 1 + \frac{d(\Delta H_{PA})}{d(DPE)} + \frac{d(E_{int})}{d(DPE)} - \frac{d(\Delta H_{ads})}{d(DPE)} \quad (8)$$

The slopes for 1-butanol (0.13) and 2-butanol (0.11) dehydration and for *n*-hexane isomerization (0.32) (Figures 4 and 5) indicate that isomerization is more sensitive to acid strength than dehydration of these two alkanols. These differences must reflect the effects of DPE on properties of reactants or transition states that influence, in turn, one or more of the terms in eq 8.

ΔH_{PA} describes reactions of molecules with protons in the gas phase and, as a result, cannot depend on any property of a solid acid ($(d(\Delta H_{PA}))/(d(DPE)) = 0$); thus, eq 8 becomes:

$$\frac{d(E_a)}{d(DPE)} = 1 + \frac{d(E_{int})}{d(DPE)} - \frac{d(\Delta H_{ads})}{d(DPE)} \quad (9)$$

indicating that DPE effects on activation barriers (Figure 5) reflect concomitant changes in E_{int} and ΔH_{ads}. The data in Figure 5 indicate that $d(E_{int} - \Delta H_{ads})/d(DPE)$ values are negative and insensitive to DPE, but differ for dehydration and isomerization reactions. These trends may reflect a decrease in E_{int} (more exothermic), an increase in ΔH_{ads} (less exothermic), or a combination of these, as acids become weaker (and DPE increases). As acids weaken, either cationic fragments at the transition state are stabilized more effectively by the anionic conjugate base or the adsorbed species leading to the transition state become less stable. The magnitude of these effects depends on the specific reactants and their reactions; as a result, slopes are smaller than unity, but are likely to differ among acid-catalyzed reactions (Figure 5).

Table 5. Deprotonation Energy (DPE), Adsorption Enthalpies ΔH_{ads}, Gas-Phase Reactant Proton Affinities (ΔH_{PA}), and Ion-Pair Interaction Energies E_{int}[d] on 0.04H_3PW/Si (See also Scheme 3)

	kJ mol^{-1}			
	DPE[a]	ΔH_{ads}[b]	ΔH_{PA}	E_{int}[d]
2-butanol elimination	1087	−77[b]	−713[c]	−343
1-butanol elimination	1087	−77[b]	−675[c]	−346
n-hexane isomerization	1087	−118	−770	−306

[a] DFT results (cf., refs 4 and 19). [b] DFT results (cf., refs 4 and 19). [c] See ref 4 and references therein. [d] $E_{int,i} = E_{a,i}$ (from Table 3) − DPE + $\Delta H_{ads,i} - \Delta H_{PA,i}$.

sec-Hexoxide isomerization activation barriers (129 kJ mol^{-1}) on $H_3PW_{12}O_{40}/SiO_2$ are much larger than for elimination from H-bonded 2-butanol intermediates (108 kJ mol^{-1}), but are more similar to the barrier for elimination from H-bonded 1-butanol (119 kJ mol^{-1}) (Table 5). The similar sensitivities for 1-butanol and 2-butanol dehydration to acid strength (DPE), despite their very different activation barriers, show that more demanding reactions are not necessarily more sensitive to acid strength than those involving more stable ion-pairs at transition states. The different activation barriers for 2-butanol and 1-butanol dehydration predominantly reflect the different ΔH_{PA} (Scheme 3) of their respective gas-phase protonation events (eq 4). ΔH_{PA} is more negative for 2-butanol (Table 5) than for 1-butanol, because secondary carbenium ions for 2-butanol are more stable than primary species for 1-butanol reactions. These different carbenium ion stabilities influence activation barriers (eq 3), but not their dependence on DPE, and they account for differences in their reaction rates and activation barriers (Figure 5).

In section 3.4, we showed that K_{prot} values increased only slightly as DPE increased (Figure 6), suggesting that ΔH_{prot} values are slightly more negative on weaker acids (Table 4) and that adsorbed precursors to isomerization transition states become more stable as acids weaken ($(d(\Delta H_{ads}))/(d(DPE)) < 0$). Thus, ΔH_{ads} ($=\Delta H_{prot}$) terms in eq 9 cannot account for the attenuated effects of DPE on activation barriers. On the contrary, this trend would increase the observed sensitivity of isomerization barriers to DPE by stabilizing reactants more effectively on weaker acids and causing an even greater increase in activation barriers than expected from a concomitant increase in DPE. In such cases, $(d(E_{int}))/(d(DPE))$ in eq 9 has to become even more negative for weaker acids than when ΔH_{prot} does not depend on acid strength to account for the trends in Figure 5.

DFT methods suggest that hydrogen-bonded alkanols leading to transition states for 2-butanol dehydration become less stable as $H_{8-n}X^{n+}W$ POM acids become weaker ($(d(\Delta H_{ads}))/(d(DPE)) > 0$).[23] Reactant adsorption can therefore attenuate, at least in part, DPE effects on elimination barriers, in contrast with the case for alkoxide isomerization. The resulting opposite signs for $(d(\Delta H_{ads}))/(d(DPE))$ in isomerization (more stable reactants on weaker acids) and dehydration (more stable reactants on stronger acids) may contribute to the different sensitivities to DPE for these two reactions. Stronger effects of DPE and ΔH_{ads} are expected for H-bonded intermediates than for covalently bound species, for which factors other than DPE govern the effects of catalyst composition on ΔH_{ads} (vide infra, section 3.4). DPE effects on reactant adsorption, however, cannot account for the weak effects of DPE on activation barriers. The slopes for the data shown in Figure 5 for elimination and isomerization (0.11 and 0.32, respectively) are much smaller than those

(36) Grimme, S. *J. Comput. Chem.* **2004**, *25*, 1463, and references therein.
(37) de Gauw, F. J. M. M.; van Grondelle, J.; van Santen, R. A. *J. Catal.* **2002**, *206*, 295.

expected if adsorption effects were solely responsible for their deviation from unity[38] (0.89 and 1.04, respectively), but may account, in part, for the different slopes observed for isomerization and dehydration reactions.

In view of the weak effects of DPE on reactant stabilization by adsorption, we consider instead how DPE may affect electrostatic stabilization of ion-pairs at transition states, a ubiquitous feature of acid catalysis. In doing so, we use a simplified form of eq 9.

$$\frac{d(E_a)}{d(DPE)} = 1 + \frac{d(E_{int})}{d(DPE)} \qquad (10)$$

in which $(d(E_{int}))/(d(DPE))$ is negative for all reactions (Figure 5), and activation barriers become increasingly sensitive to DPE as its value approaches zero.

Compensation between E_{int} and DPE becomes evident upon deconvolution of deprotonation and stabilization processes into their constituent elementary steps within thermochemical cycles. In deprotonation, thermochemical cycles would consider protons and anions to form via homolytic cleavage of H−A bond (BE(HA)) and subsequent transfer of an electron from H-atoms to the base (E_{trans}), while preserving the location of all atoms involved:

$$\text{Step 1: } H{-}A \rightarrow H^+ \cdots A^- \quad BE(HA) + E_{trans} \qquad (11)$$

E_{trans} reflects the sum of the ionization potential of a hydrogen atom, the electron affinity of the neutral cluster, and the energy gained by the interaction of the proton with the anionic conjugate base (vide infra). Next, protons and anions are brought apart by overcoming their electrostatic stabilization, at an energy cost of $-E_{int,H+}$:

$$\text{Step 2: } H^+ \cdots A^- \rightarrow H^+ + A^- \quad -E_{int,H+} \qquad (12)$$

$E_{int,H+}$ contains electrostatic stabilization, as well as the energy required to reorganize charge from that in the isolated anions to that present when interacting with the proton. $E_{int,H+}$ is the predominant component in DPE values;[39] it becomes more negative as acids weaken.

$E_{int,H+}$ and E_{int} reflect electrostatic stabilization in thermochemical cycles for protons and cationic molecules, respectively, with the same singly charged anionic cluster. Weaker acids form less stable and more densely charged conjugate bases upon deprotonation,[23] which also stabilize cations more effectively than those in stronger acids. Keggin POM clusters of uniform size become more densely charged as their DPE values increase (e.g., with increasing number of protons).[4] As a result, higher DPE values (in weaker acids) are compensated by the greater concomitant stabilization of ion-pairs at the transition state as compared to clusters with smaller DPE values (stronger acids). The part of the DPE values recovered by ion-pair stabilization depends on how anionic clusters interact with the more localized charge of the proton as compared to the more diffuse charges in the organic cations at the transition state. Localized charges at cationic transition states, which resemble protons in their electrostatic interactions, would interact most effectively with the anionic cluster and recover a larger fraction of the energy required to deprotonate the acid than organic cations with a more diffuse positive charge (Scheme 4).

Scheme 4. Energy Diagram Showing the Relative Magnitudes of Electrostatic Stabilization for a Proton ($E_{int,H+}$), the 2-Butanol Dehydration Transition State ($E_{int,but}$), and the *n*-Hexane Isomerization Transition State ($E_{int,hex}$) by an Anionic Conjugate Base[a]

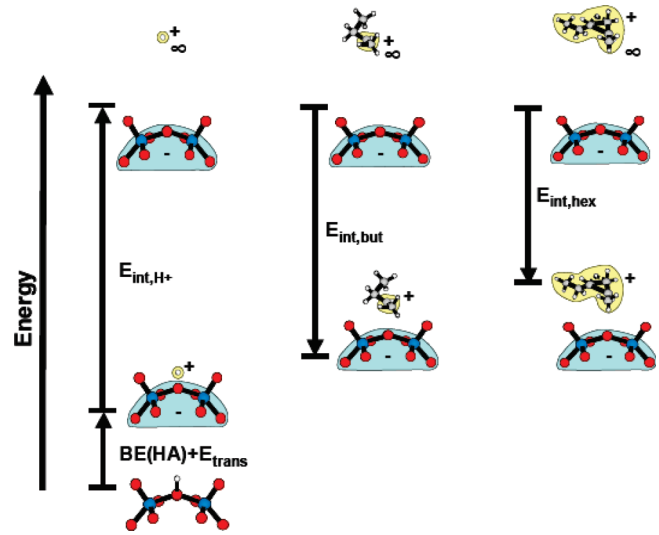

[a] Stabilization increases with increasing charge localization ($|E_{int,H+}| > |E_{int,but}| > |E_{int,hex}|$). "∞" denotes cationic species that are not interacting with the conjugate base.

We consider first ion-pairs as point charges,[40] for which electrostatic interactions are given by:

$$E_{elec} = \sum_a \sum_c \frac{q_a q_c}{4\pi\varepsilon_0 r_{ac}} \qquad (13)$$

E_{elec} becomes more negative (and ion-pairs more stable) as the distance (r_{ac}) between the positive (q_c) and negative (q_a) charges decreases. As charge density increases in the anion, stabilization of a given cation (e.g., carbenium ion, proton) increases and attenuates DPE effects on activation barriers. In the same manner, a higher charge density in organic cations leads to more effective stabilization by the conjugate base. The charge density is greatest and the charge separation (r_{ac}) smallest for protons, which lack core electrons; as a result, $E_{int,H+}$ values are most negative for protons. Ion-pairs at transition states cannot fully recover the energy required to remove protons, but do this to a greater extent for small cations with localized charge (Scheme 4); these small, highly charged cations lead to weaker DPE effects on activation barriers because they recover a larger fraction of the energy used to deprotonate the acid than do cations with more diffuse charge and with greater charge separation. As a result, reactions involving diffuse positive charges in the ion-pair will be more sensitive to acid strength. A specific example of the effects of charge distribution on the stability of the ion-pair is included in the Supporting Information; in this example, an equation for $d(E_{int})/d(DPE)$ is derived using the two-step deprotonation process (eqs 11 and 12) and the point-charge model (eq 13).

A point-charge description of electrostatic interactions neglects the energy required to redistribute charge densities as ions approach each other, but free carbenium ions may perturb their optimal charge distributions as gas-phase species to interact

(38) Here, deviations from unity by adsorption $((d(\Delta H_{ads}))/(d(DPE)))$ were calculated using values of ΔH_{ads} estimated from measured K_{prot} values (Figure 6) and calculated pre-exponentials (Table 4) for *n*-hexane isomerization, and from the DFT calculations in ref 20 for 2-butanol dehydration. The values of slopes shown were calculated by $1 + (d(\Delta H_{ads}))/(d(DPE))$.

(39) DFT calculations for H_2SO_4 with a DPE of 1315 kJ mol^{-1} suggest a value of 356 kJ mol^{-1} for E_{reorg} and 959 kJ mol^{-1} for $-\Delta E_{int,H+}$.

(40) Strittmatter, E. F.; Williams, E. R. *Int. J. Mass Spectrom.* **2001**, *212*, 287.

Scheme 5. Point-Charge Model To Illustrate the Changes in the Charge Distribution upon Formation of the Kinetically Relevant Edge-Protonated Dialkyl Cyclopropyl Transition State (b) from the Secondary Carbenium Ion (a)[a]

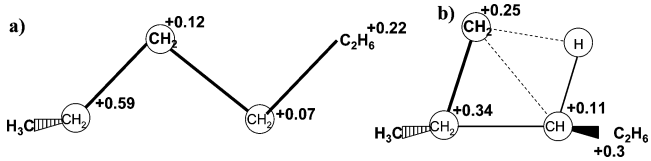

[a] The DFT-calculated Mulliken atomic charges of the respective CH_x fragments are denoted as, for example, +0.34 (at the top right of the CH_x fragment).

most effectively with charges in the anion. This redistribution energy is compensated by stronger electrostatic interactions that minimize the total ion-pair energy. Polarizable cations that localize charge without large energy requirements and those with high intrinsic charge densities will interact most effectively with anions at these transition states.

These concepts are reminiscent of those embedded within hardness−softness acid−base (HSAB) theory,[41] widely used to describe the behavior of Lewis acids and bases in the liquid phase. Soft species have diffuse or polarizable electron clouds, while hard species have localized charges. Hard−hard interactions form stable ionic species, because of strong electrostatic interactions at the small distances favored by the localized charges. Soft acids and bases form covalent complexes instead of ion-pairs. Increasing the hardness of either the acid or the base forms more stable ion-pairs. Protons are small and highly charged and, as one of the hardest Lewis acids, interact most strongly with a given base. Organic cations at transition states are softer (more diffuse charge) than protons and exploit electrostatic stabilization less effectively. These arguments and the effects of DPE on activation barriers (Figure 5) suggest that elimination transition states have a higher local charge density than do isomerization transition states; as a consequence, they recover a larger fraction of the energy required for deprotonation and give activation barriers that are less sensitive to acid strength than for isomerization reactions.

These conclusions are consistent with the charge distributions for isomerization and elimination transition states inferred from DFT treatments. The Mulliken atomic charge[42] at the sp_2 carbon in gas-phase linear *sec*-hexyl carbenium ions (Scheme 5a), which resemble carbenium ions involved in 2-butanol dehydration transition states,[23] is +0.59. The charge in the sp_2 carbon in edge-protonated dialkyl-cyclopropyl species (Scheme 5b), which resembles those in isomerization transition states,[43] is smaller (+0.34), and the rest of the net +1 charge is delocalized throughout the rest of the molecule. The more diffuse charge in edge-protonated dialkyl-cyclopropyl species (Scheme 5b) as compared to secondary carbenium ions in elimination reactions (Scheme 5a) leads to less effective stabilization and recovers a smaller fraction of the energy required to remove the protons from the acid.

Experimental E_{int} values for *n*-hexane isomerization and for 2-butanol and 1-butanol dehydration on $H_3PW_{12}O_{40}/SiO_2$ are shown in Table 5. These estimates were obtained from experimental alkanol dehydration[4] and alkane isomerization

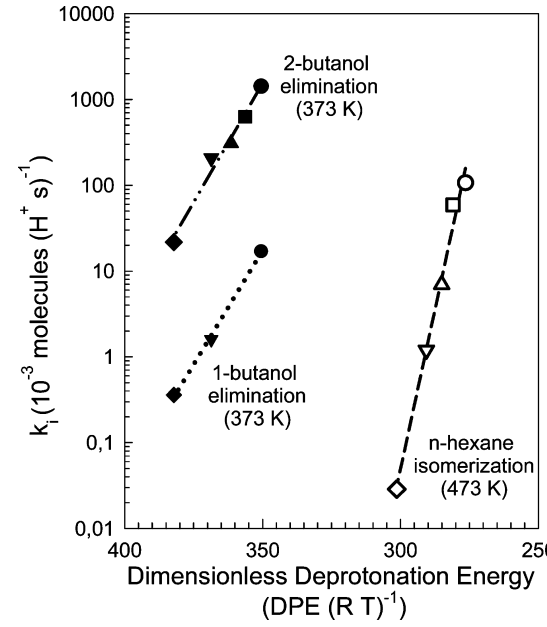

Figure 7. 1-Butanol dehydration rate constants k_{elim} (full symbols) and as a function of the normalized deprotonation energy (DPE $(RT)^{-1}$) for $0.04H_3PW/Si$ (●), $0.04H_6CoW/Si$ (▼), and H-BEA (◆) (373 K). For comparison, the 2-butanol dehydration rate constant (373 K) (see refs 1 and 4) are also shown (full symbols), and the isomerization rate constants k_{isom} (open symbols) (from Figure 4) as a function of (DPE $(RT)^{-1}$) (dashed line) are also shown. 95% confidence intervals for rate constants from regression are $<\pm 6.5\%$ of the reported values.

barriers (section 3.3), alkanol adsorption enthalpies from DFT,[23] measured *n*-hexene protonation enthalpies (section 3.4), DPE values from DFT,[1] and measured thermodynamic data for elimination ΔH_{PA}[10,44,45] (eq 4), and isomerization ΔH_{PA} from DFT (eq 5). E_{int} values are much less negative for isomerization (−306 kJ mol^{-1}) than for 2-butanol (−343 kJ mol^{-1}) or 1-butanol (−346 kJ mol^{-1}) dehydration (Table 5), indicating that ion-pairs are more effectively stabilized in elimination than in isomerization transition states. These data confirm that for localized anionic charges, cations with a diffuse charge, prevalent at isomerization transition states, are less effectively stabilized and lead to less negative E_{int} values and a stronger dependence of activation barriers on acid strength.

3.6. Assessing the Sensitivity of Reactions to Acid Strength Based on Elementary Step Rate and Equilibrium Constants. Some activation barriers cannot be assessed on the basis of the approach in section 3.3, because their transition state geometries or pre-exponential factors are uncertain. For such reactions, we must assess their sensitivity to DPE based solely on measured rate constants. For pre-exponential factors that depend weakly on DPE, the effect of DPE on rate constants is given by:

$$\frac{d(\ln(k))}{d(DPE)} = -\frac{1}{RT}\frac{d(E_a)}{d(DPE)} \qquad (14)$$

and $\ln(k)$ depends linearly on (DPE/*RT*) with a slope that gives the sensitivity to acid strength defined by eq 9.

Figure 7 shows 1-butanol and 2-butanol dehydration and *n*-hexane isomerization rate constants (k_i) on $H_{8-n}XW$ (X = P^{5+}, Si^{4+}, Al^{3+}, and Co^{2+}) and H-BEA as a function of

(41) Ayers, P. W.; Carr, R. G.; Pearson, R. C. *J. Chem. Phys.* **2006**, *124*, 194107.
(42) Here, the charges on the hydrogen atoms are condensed into the heavy atoms.
(43) Neurock, M., unpublished results.
(44) Aue, D. H.; Bowers, M. T. *Gas Phase Ion Chemistry*; Academic Press: New York, 1970; Vol. 2, p 32.
(45) Hunter, E. P. L.; Lias, S. G. *J. Phys. Chem. Ref. Data* **1998**, *27*, 413.

dimensionless deprotonation enthalpies (DPE/*RT*).[1,4] The slopes in Figure 7 for 1-butanol and 2-butanol dehydration are similar and significantly smaller than for *n*-hexane isomerization rate constants, as also concluded from activation barriers (Figure 5).

More demanding acid-catalyzed reactions do not, in general, depend more sensitively on acid strength. Rate constants are lower for *n*-hexane isomerization with cyclic transition states and low activation entropies than for elimination reactions with late transition states and high activation entropies, merely because pre-exponential factors are much smaller in the former. The higher pre-exponential factors for alkanol dehydration reactions, and not the greater stability of its transition state, account for the lower temperature required (343−373 K) as compared to *n*-hexane isomerization (473 K). In fact, barriers for 1-butanol dehydration and *n*-hexane isomerization are nearly identical on $H_3PW_{12}O_{40}/SiO_2$; yet *n*-hexane isomerization barriers and rate constants are much more sensitive to acid strength than those for 1-butanol dehydration reactions.

We conclude that the sensitivity of a given reaction to acid strength predominantly reflects the extent to which electrostatic interactions at the transition state ion-pair become more effective (and E_{int} becomes more negative) as the strength of the acid sites decreases (DPE increases). This trend reflects the ability of transition states to recover, in part, the energy required to remove the proton from the conjugate base, which depends predominantly on the electrostatic stabilization of the proton by the conjugate base. It is also plausible that different sensitivities of dehydration and isomerization reactions are partly because of their opposite adsorption enthalpy trends as acid strength increases. POM clusters and acid zeolites form conjugate bases that interact most effectively with cations with localized charges. The hardness of transition states, determined by the extent to which charges are as localized as in protons, determines the extent to which deprotonation energies are recovered by electrostatic stabilization of the ion-pair transition states. Dehydration reactions depend less sensitively on acid strength apparently because of the more localized nature of the positive charge in their transition state as compared to those relevant in alkane isomerization reactions.

Conclusions

Alkane isomerization and alkanol dehydration rates, measured on Keggin polyoxometalates (POM) and zeolites, are used to demonstrate how acid-catalyzed reactions sense acid strength, which is rigorously described by deprotonation energies (DPE) for these well-defined structures and varied by changing their compositions. *n*-Hexane isomerization rates measured on these solid acids as physical mixtures with Pt/A_2O_3 that maintain alkane−alkene equilibrium depend on the rate constant for skeletal isomerization of *sec*-hexoxides, the equilibrium constant for *n*-hexane dehydrogenation to *n*-hexene isomers, and the equilibrium constant for the formation of *sec*-hexoxides from linear *n*-hexene isomers, and are only a function of the molar (*n*-hexane/H_2) ratio. Rates were normalized by the number of accessible catalytic acid sites measured by titration during catalysis using 2,6-di-*tert*-butylpyridine. The elementary isomerization rate constants decreased exponentially with increasing DPE values, a result previously reported for alkanol dehydration reactions. This dependence shows that acid strength predominantly affects activation barriers and is consistent with rigorous thermochemical cycles of activation barriers in terms of reactant, catalyst, and ion-pair properties. Isomerization activation barriers exhibit a stronger dependence on DPE than those for alkanol dehydration, and all reactions have barriers that increase less than concomitant increases in DPE values.

Similar sensitivities of 1- and 2-butanol barriers to DPE despite largely different values demonstrate that reaction difficulty is predominantly dictated by reactant proton affinities that form the respective transition states and is not necessarily indicative of a reaction's sensitivity to acid strength. Hexene protonation equilibrium constants show increasing stability of alkoxides on weakening acids, while calculations of alkanol adsorption by hydrogen bonding show the opposite trend, which may account for part of the difference between the reactions' sensitivities. These effects are small, however, compared to changes in electrostatic stabilization of ion-pair transition states among different acids. Weaker acids have more densely charged conjugate bases that stabilize protons and transition states more than do stronger acids; however, the localized charge of protons interacts most effectively with the anionic charge, leading to only partial energy recovery by transition states. Transition states with localized charges are able to recover more of the deprotonation energy than those with diffuse charges and therefore are less sensitive to acid strength. Thus, the elimination transition state, whose positive charge is denser than that for isomerization, is stabilized more by the conjugate base, leading to its lower sensitivity.

Acknowledgment. We acknowledge with thanks many technical exchanges with Professor Matthew Neurock (University of Virginia), whose contributions to the theoretical treatment of POM clusters and their acid strength were instrumental to the concepts extended in this Article. The financial support by the Chemical Sciences, Geosciences, and Biosciences Division, Office of Basic Energy Sciences, Office of Science, U.S. Department of Energy, under grant number DE-FG02-03ER15479 is gratefully acknowledged. We also thank Dr. Cindy Yin (UC Berkeley) and Dr. Stuart L. Soled (ExxonMobil) for their assistance with the synthesis of bulk H_5AlW and H_6CoW polyoxometalate clusters.

Supporting Information Available: Equations for $d(E_{int})/d(DPE)$ dependence on charge distributions; complete ref 11. This material is available free of charge via the Internet at http://pubs.acs.org.

JA900829X